Kinetic Modeling of mant-ATP Turnover to Interpret the Biochemically Defined Myosin Super-Relaxed State

Filip Ježek[1,3], Seungyeon Julia Han[2], Alison S. Vander Roest[2], Daniel A. Beard[1*]

1 Department of Molecular and Integrative Physiology, University of Michigan, Ann Arbor, Michigan, USA
2 Department of Biomedical Engineering, University of Michigan, Ann Arbor, Michigan, USA
3 Department of Pathological Physiology, First Faculty of Medicine, Charles University, Prague, Czechia

* beardda@umich.edu

Abstract

The fluorescent ATP analog mant-ATP has become a valuable tool for quantifying occupancy of the myosin super-relaxed (SRX) state, a biochemically inactive conformation of myosin in striated muscle. Interpretation of mant-ATP fluorescence decay kinetics is confounded by inconsistencies in state definitions and kinetic assumptions. Here, we develop a mass-action kinetic model of myosin cross-bridge cycling and mant-ATP turnover to reconcile these discrepancies and provide a mechanistic framework for interpreting SRX measurements. Our model simulates ATP label-chase experiments and demonstrates that conventional double-exponential fitting methods do not directly quantify SRX occupancy. Instead, we show that slow and fast decay phases of mant-ATP fluorescence arise from label redistribution among kinetically distinct states, not state populations in equilibrium. The model resolves several apparent paradoxes identified in recent studies by reproducing experimental observations without requiring SRX and DRX kinetic isolation or implausible equilibrium constants. Simulations further quantify the impact of experimental factors—such as ADP accumulation, photobleaching, and initial rigor state occupancy—on fluorescence kinetics and SRX estimates. These results support a revised framework for SRX quantification and suggest that label-chase experiments must be interpreted using mechanistic models to accurately assess myosin state distributions and transition kinetics.

Author summary

1 Introduction

Experiments using the fluorescent ATP analog 2'/3'-O-(N-Methyl-anthraniloyl)-adenosine-5'-triphosphate (mant-ATP) have been used since 2010 to interrogate the biochemical state of myosin in intact muscles. Stewart et al. [1] introduced the technique of following the kinetics of mant-ATP binding and unbinding to quantify the proportion of myosin in the super-relaxed (SRX) state in a rabbit skeletal muscle preparation. Together with the experiments of Hooijman et al. [2], which were the first to apply this approach to cardiac

muscle, these studies were instrumental in the the identification of the SRX as a distinct biochemical state of myosin. While a consensus has emerged on the existence of the SRX state, its structural basis—particularly its association with the interacting-heads motif (IHM) conformation—remains debated [3]. Craig et al. have suggested that the biochemically defined SRX state is strongly related or even equivalent to the structural myosin conformation of the interacting head motif (IHM) [4,5]. Others suggest that the structurally defined IHM and biochemically defined SRX states do not necessarily reflect functionally related states and that these states are rarely established simultaneously [3,6] Thus, it remains and open question as to whether or not the SRX population corresponds to the IHM population. Indeed, the interpretation of exactly how the observed mant-ATP kinetics reflect the biochemical/structural state of myosin is not entirely certain [6].

In a typical, microscope-based mant-ATP protocol, a permeabilized muscle or myofibril isolate is first incubated for several minutes or hours in ATP-containing solution [1] and then washed with rigor buffer containing no ATP [2]. Next, the muscle is incubated for several minutes with low concentration of mant-ATP (e.g., 250 μM for 2 minutes [2]). The labeled mant-ATP is then chased with a higher concentration of unlabeled ATP (usually 4 mM), while observing the fluorescence intensity. Since the mant-ATP shows substantially increased fluorescence in the bound state, the observed decay of fluorescence during the chase phase is interpreted to reflect the kinetics of mant-ATP (or mant-ADP) unbinding from myosin. Moreover, the kinetics of replacement of the labeled mant-ATP with unlabeled ATP is interpreted to reveal distinct populations of myosin, representing the SRX and the disordered relaxed (DRX) state. Specifically, the SRX state is associated with a relatively slower decay of mant-ATP fluorescence in a buffer solution containing unlabeled ATP.

The observed intensity decay $I_{obs}(t)$ is normalized and fit to a double exponential function, in the form of either Equation (1) [1,2] or Equation (2) [6,7]):

$$\begin{aligned} I(t) &= \frac{1 - C_{fast}\left(1 - e^{-t/T_{fast}}\right) - C_{slow}\left(1 - e^{-t/T_{slow}}\right)}{I_{max}} \\ SRX_{est} &\approx C_{slow} \end{aligned} \tag{1}$$

$$\begin{aligned} I_{obs}(t) &= \frac{C_{fast}(e^{-t/T_{fast}}) + C_{slow}(e^{-t/T_{slow}}) + I_{bg}}{I_{max}}, \\ SRX_{est} &\approx \frac{C_{slow}}{C_{fast} + C_{slow}} \end{aligned} \tag{2}$$

where I_{max} is maximal measured intensity during the incubation or chase phase (protocols differ) and I_{bg} is a background intensity constant. The relative occupancy of the SRX state, SRX_{est}, is estimated as the amplitude of the slower phase (Equation (1) in Hooijman et al. [2]) or proportional to the slower phase (Eq. 2, as in [2]), with $T_{slow} \gg T_{fast}$ and T_{slow} typically > 100 s. For example, Hooijman et al. report $T_{slow} = 144 \pm 10$s in cardiac muscle [2].

Mohran et al. [6] recently highlighted three critical paradoxes associated with the interpretation of these experiments. The first is that if the SRX and DRX states are maintained in thermodynamic equilibrium, and are able to freely interconvert on a time scale faster than the replacement of mant-ATP by unlabeled ATP in the chase phase of the experiment, then the bound mant decay would follow a single exponential. Two distinct decay processes with different time scales would follow only if the SRX and DRX states are

"kinetically isolated" on the timescale of the experiment, the two exponential decay function representing the proportions of myosin in the SRX and DRX states. Second, Mohran et al. point out that steady-state ATPase assays often disagree with SRX population estimates. For example, Gollapudi et al. observed that the myosin inhibitor mavacamten inhibits ATPase activity by only 70% while supposedly increasing the SRX population to effectively 100%—a mismatch that challenges the biochemical definition of SRX [8, 9]. A third paradox follows from observations of Walklate et al. [7], who report that SRX formation becomes detectable after only 200 ms of incubation with mant-ATP, yet seemingly requires hundreds of seconds to decay. This observation suggests an equilibrium mass action ratio that would overwhelmingly favor the SRX state, in conflict with interpretation of data using Equation (1) or Equation (2). The relatively fast loading of mant-ATP into the SRX state is also in apparent conflict with the requirement that the SRX and DRX states remain "kinetically isolated" on the timescale of the mant-ATP fluorescence decay.

To help resolve these paradoxes we have developed a kinetic model for mant-ATP tracer label kinetics based on a simple multi-state model of the cross-bridge cycle and SRX/DRX transitions. The goal is to develop a kinetic model that integrates the biochemical, structural, and functional observations to resolve inconsistencies and provide a unified mechanistic framework for quantification of SRX state kinetics. It is demonstrated that the three paradoxes of Mohran et al. are resolved based on a simple kinetic model. Specifically, model analysis shows that there is little mechanistic correspondence between the magnitude of a slower versus faster decay phase as assessed by either Equation (1) or Equation (2) and the relative occupancy of SRX and DRX states of myosin. In addition, our analysis provides a means of quantitatively estimating state occupancy probabilities and transition rate constants from the mant-ATP label/chase experiment.

2 Methods

2.1 Computational Model

Our analysis is based on the simple kinetic model illustrated in Figure 1, similar to models of the myosin-actin crossbridge cycle developed by this and other groups [10–12]. In the model myosin exists in the SRX state (labeled S), one of two unattached DRX states (labeled D_T and D_D), or one of two attached states (A_1 and A_2). The SRX state S interconverts with the ATP-bound DRX state D_T with transition rates proportional to first-order rate constants k_S and k_{D_T}. The transition from D_T to D_D involves hydrolysis of the bound ATP and thus the transition back from D_D to D_T involves exchange of the bound ADP for an ATP molecule from the buffer. The transition from D_T to D_D is part of the canonical cross-bridge cycle and is typically found to be relatively rapid (associated with a time constant of less than a second). Combining the forward transition from D_T to D_D with the reverse transition from D_D to D_T represents a net ATP hydrolysis that is associated with no cross-bridge attachment, force development, or work. This futile cycle is expected to be relatively slow—operating on a time scale of many seconds. Consistent with the crossbridge models we hypothetize, it is via this step that unlabeled ATP replaces the labeled fluorophore in the chase phase of the experiments simulated below.

The states A_1 and A_2 represent myosin bound to actin. The A_2 state represents actin-bound myosin in the post-ratcheted rigor state (sometimes called the strongly bound state). The A_1 state is the pre-ratcheted or weakly bound state. In the experiments analyzed here it is assumed that the A_1 state is never sampled. However, in the initial rigor state, with no ATP present the system, the myosin is able to

exist in the attached A_2 state.

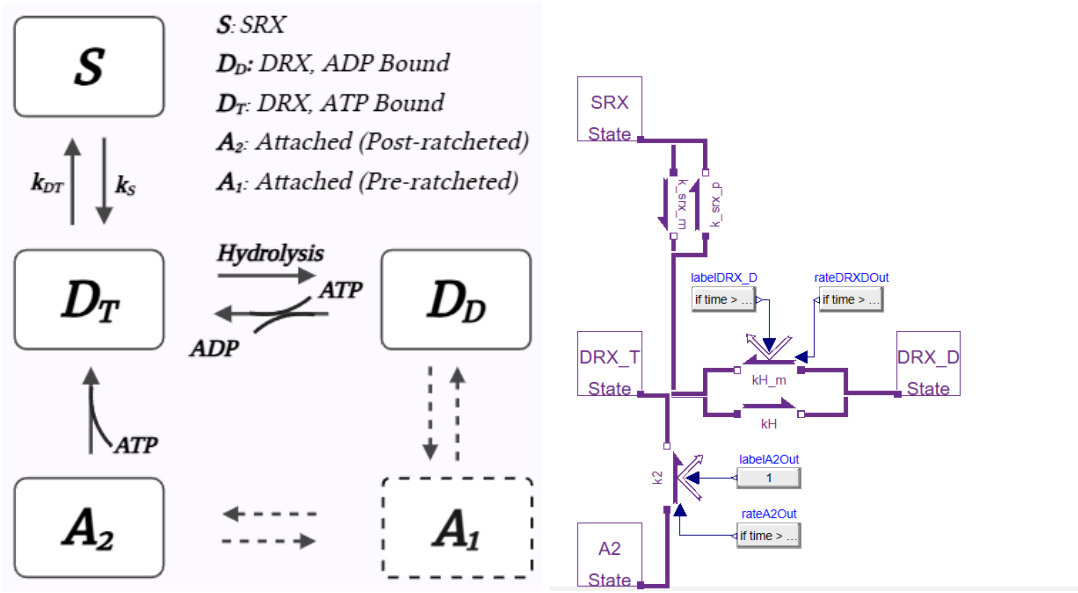

Fig 1. a) Schematic mathematical model. b) Schematic of Modelica implementation of mathematical model with population labeling. The filled half-arrows represent kinetic first-order transitions, the empty bounce-back arrows mark the transition exchanges the ATP, which leads to labeling (incubation phase) or unlabeling (chase phase) of the population flow.

The probability of each state (equivalent to the relative occupancy) is denoted P_x, where x represents a given state. Ignoring the A_1 state we have:

$$\sum P_x = P_{\mathrm{S}} + P_{\mathrm{D_T}} + P_{\mathrm{D_D}} + P_{\mathrm{A_2}} = 1\,.$$

To simulate an experimental protocol where the system is initially incubated in an ATP-free rigor solution, the state probabilities are governed by the following system of equations

$$\begin{aligned}
\frac{dP_S}{dt} &= -k_S P_S + k_{D_T} P_{D_T} \\
\frac{dP_{D_T}}{dt} &= \begin{cases} +k_S P_S - k_{D_T} P_{D_T} - k_H P_{D_T}, & \text{if } t < T_{\text{incubation}} \\ +k_S P_S - k_{D_T} P_{D_T} - k_H P_{D_T} + \hat{k}_{D_D} P_{D_D} + k_{A2} P_{A_2}, & \text{otherwise} \end{cases} \\
\frac{dP_{D_D}}{dt} &= \begin{cases} +k_{D_T} P_{D_T}, & \text{if } t < T_{\text{incubation}} \\ +k_{D_T} P_{D_T} - \hat{k}_{D_D} P_{D_D}, & \text{otherwise} \end{cases} \\
\frac{dP_{A_2}}{dt} &= \begin{cases} 0, & \text{if } t < T_{\text{incubation}} \\ -k_{A2} P_{A_2}, & \text{otherwise} \end{cases} .
\end{aligned} \tag{3}$$

Here is assumed that during an initial rigor phase ($t < T_{\text{incubation}}$) there is no transition $D_D \to D_T$ or $A_2 \to D_T$ because no ATP is present.

Model analysis of the mant-ATP tracer kinetic experiment tracks the fraction of each ATP/ADP-bound state that is bound to the fluorescent mant-ATP/ADP label. We define F_x as the fraction of each state that has the mant label on the attached ATP/ADP, and the total probability that a myosin head has a mant label attached as $M_x = F_x P_x$. From these definitions we have

$$\begin{aligned}
\frac{dM_S}{dt} &= -k_S M_S + k_{D_T} M_{D_T} \\
\frac{dM_{D_T}}{dt} &= +k_S M_S - k_{D_T} M_{D_T} - k_H M_{D_T} + Q_{A_2} + Q_{D_D} \\
\frac{dM_{D_D}}{dt} &= +k_{D_T} M_{D_T} - \hat{k}_{D_D} M_{D_D} \,. \qquad (4)
\end{aligned}$$

and finally, simulated fluorescence intensity of the label I_{sim} is calculated as a normalized sum of M_x plus observed background I_{bg}:

$$M_{tot} = M_S + M_{D_T} + M_{D_D} \qquad (5)$$

$$I_{sim} = \frac{M_{tot}}{I_{max} - I_{bg}} + I_{bg} \qquad (6)$$

The governing equations for the mant- label, Equation (4), are coupled to the equations governing the bulk probabilities, Equation (3), via the terms Q_{A_2} and Q_{D_D}, which determine the rate at which the label is added to myosin. The rate $Q_{A_2}(t)$ is the rate of addition of mant-ATP associated with the transition $A_2 \to D_T$ and $Q_{D_D}(t)$ is the rate of addition of mant-ATP asociated with the transition $D_D \to D_T$:

$$Q_{A_2} = \begin{cases} 0, & \text{if } t < T_{\text{incubation}} \\ k_{A_2} P_{\text{A}_2}, & \text{if } T_{\text{incubation}} \leq t \leq T_{\text{chase}} \\ 0, & \text{if } t > T_{\text{chase}} \end{cases} \qquad (7)$$

$$Q_{D_D} = \begin{cases} 0, & \text{if } t < T_{\text{incubation}} \\ \hat{k}_{D_D} P_{\text{D}_\text{D}}, & \text{if } T_{\text{incubation}} \leq t \leq T_{\text{chase}} \\ 0, & \text{if } t > T_{\text{chase}} \end{cases} \,. \qquad (8)$$

As above, we assume that during the initial rigor phase ($t < T_{\text{incubation}}$) there is no mant-ATP present and thus $Q_{D_D} = Q_{A_2} = 0$. During the incubation phase ($T_{\text{incubation}} \leq t \leq T_{\text{chase}}$) mant-ATP is loaded onto myosin at the rates $k_{A_2} P_{\text{A}_2}$ and $\hat{k}_{D_D} P_{\text{D}_\text{D}}$. For simulations accounting for ADP-mediated inhibition $\hat{k}_{D_D}$ is an apparent rate constant that depends on ADP concentration, as described below in Section 2.1.2. Otherwise $\hat{k}_{D_D}$ is a constant independent of reactant concentrations.

2.1.1 Photobleaching

The fluorescence intensity of mant-ATP decreases over time due to degradation of the mant group by the applied excitation energy. To simulate photobleaching under conditions of steady incident light intensity the mant signal intensity is assumed to decay exponentially

$$\hat{M}_{tot}(t) = M_{tot}(t) e^{\frac{-(t - T_{incubation})}{\tau_{pb}}} \qquad (9)$$

where the corrected total active mant-label $\hat{M}_{tot}(t)$ replaces the $M_{tot}(t)$ in Equation (6) and τ_{pb} is a photobleaching time constant.

2.1.2 ADP-Mediated Inhibtion

The Q_{DD} transition involves release of bound ADP and thus may be influenced by ADP concentration, particularly at relatively high concentrations of myosin/myofibrils or for long incubation times. The potential inhibitory effect of ADP concentration (both mant-ADP and ADP) on the $D_D \rightarrow D_T$ transition is investigated by assuming an effective rate constant for this transition, $\hat{k}_{D_D}$, influenced by C_{ADP}, the concentration of ADP in the experimental buffer:

$$\hat{k}_{D_D} = \frac{k_{D_D}}{1 + C_{ADP}/K_i}, \tag{10}$$

where K_i is an inhibition constant. The total ADP (labeled plus unlabeled) concentration is determined by the rate of turnover of the state D_D to D_T:

$$\frac{dC_{ADP}}{dt} = \frac{\hat{k}_{D_D} P_{D_D} C_M}{D}, \tag{11}$$

where C_M is the concentration of myosin ATPase in the experimental system and D is the dilution factor caused by mixing with incubation or chase solutions (rigor = incubation = 1, chase = 2 in the single mixing experiments and rigor = 1, incubation = 2, chase = 4 in double mixing experiments , as in [7]).

Variable	*Description*	*Initial value*	*Units*
P_S	SRX population	0	–
P_{D_T}	ATP-bound DRX population	0	–
P_{D_D}	ADP-bound DRX population	1-$P_{A_2,0}$	–
P_{A_2}	Attached state (rigor) population	$P_{A_2,0}$	–
M_S	Mant-ATP amount in SRX state	0	
M_{D_D}	Mant-ATP amount in DRX_D state	0	
M_{D_T}	Mant-ATP amount in DRX_T state	0	
C_{ADP}	Concentration of produced ADP*	0	mM

* Only in ADP-sensitive experiment, presented in Section 3.3

Table 1. Model state variables.

2.2 Experimental and Simulation Protocol

The kinetic model is applied to simulate mant-ATP label-chase experiments, such as those of Hooijiman et al. [2] and Walklate et al. [7], in which either permeablized fibers or myofibrils are first incubated in an ATP-free rigor solution. A mant-ATP containing solution is then introduced for an incubation period, during which the mant-ATP label binds to myosin heads. The incubation period is followed by a chase period, in which unlabeled ATP is introduced and the mant label is displaced by the unlabled ATP.

We use the convention that $t = 0$ represents the beginning of the chase phase. I.e., $T_{chase} = 0$ in the above equations. The mant-ATP incubation phase (also referred to as the "loading phase", "labeling phase"

Optimized parameters				*Value*			*Unit*
Parameter	*Description*	*Hooijman*	*Walklate*	*Walklate, RF*	*Walklate, PB*	*Walklate, AS*	
k_{D_D}†	D_D to D_T transition rate	6.9×10^{-2}	2.7×10^{-2}	2.7×10^{-2}	2.5×10^{-2}	2.9×10^{-2}	s^{-1}
k_{D_T}	D_T to SRX transition rate	4.3	9.4	8.7	10	8.9	s^{-1}
k_S	SRX to D_T transition rate	6.4×10^{-3}	4.3×10^{-3}	4.3×10^{-3}	2.0×10^{-3}	4.2×10^{-3}	s^{-1}
Fixed parameters							
k_H	Hydrolysis (D_T to D_D) transition rate ‡	80	80	80	80	80	s^{-1}
k_{A_2}†	A_2 to D_T transition rate ‡	50	50	50	50	50	s^{-1}
D_i	Incubation duration	120	60	60	60	60	s
K_i	Inhibition constant on k_{D_D} transition					0.5	μM
T_{pb}	Photobleaching time constant				500		s
$P_{A_2,0}$	Initial rigor fraction	0.4	0.4	0.8	0.4	0.4	%
I_{max}	Maximal measured fluorescence intensity	100	106	106	106	106	%
I_{bg}	Maximal measured fluorescence intensity	0.07	99	99	99	99	%

†ATP-requiring (labeling) transitions
‡Value high enough the inhibition does not apply.

Table 2. Optimized model parameters. Data from Hooijman et al. [2], Table 1 for cardiac tissue (rabbit ventricle) and Walklate et al. [7], Fig. 1, for skeletal muscle (bovine masseter). RF - Rigor fraction analysis (Section 3.4 and Fig. 6), PB - photobleaching analysis (Section 3.5 and Fig. 7), AS - ADP accumulation sensitivity analysis (Section 3.3 and Fig. 5).

or "aging time" elsewhere) is defined to begin at $t = T_{incubation}$. An initial population of cross-bridges is assumed to exist in the attached state A_2 during the initial rigor state, $A2_0 \in (0, 1)$. Since no ATP is present in the rigor state, the probability P_{A_2} remains constant at this fixed value during the rigor state. The probabilities P_S, P_{D_T}, and P_{D_D} are assumed to be in equilibrium during the rigor state, with the equilibrium distribution of states is determined by the steady-state solution to Equation (3) for $t < T_{incubation}$. For conditions simulated here, with no ATP present, $P_S = 0$, $P_{D_T} = 0$ and $P_{D_D} = 1 - A2_0$ in the rigor state.

2.3 Model Baseline Identification

Model parameters (see Table 1) k_H and k_{A2} are set to $k_H = 80$ s^{-1} and $k_{A2} = 50$s^{-1}. These values are sufficiently high that matches to experimental data are not sensitive to the values chosen. Other parameter values are estimated based on the fluorescence data of ATP chase after mant-ATP incubation experiments reported in the literature. For simulations of the experiments on rabbit ventricular muscle reported in Hooijman et al. [2], a pseudo-data set was constructed from Table 1 of Hooijman et al. [2], using Equation (1) to generate the chase-phase fluorescence time course. The sum of squared difference of simulated and observed fluorescent decay data ($\sum(I_{sim} - I_{obs})^2$) was minimized by optimizing k_{D_D}, k_{D_T}, and k_S. Estimated parameter values are listed in Table 1.

2.4 Model Implementation

The model is implemented in the Modelica language using the Bodylight v1.1 library (`https://github.com/creative-connections/bodylight.mo`) and is available on GitHub at `https://github.com/beards-lab/mant-ATP-SRX`. The model schematics is shown on Fig. 1 B. Open-source tools, such as OpenModelica, can be employed for simulation. Please see the code documentation for more information.

3 Results

3.1 Analysis of the Hooijman et al. Experiment

Fig. 2 shows a simulation of a microscope-based mant-ATP assay of rabbit ventricular muscle strips, reported by Hooijman et al. [2]. For this experiment, the mant-ATP incubation time is 2 minutes, and the initial rigor state probability is assumed to be $A2_0 = 40\%$. Parameter values for these simulations are listed in Table 2. Simulations in Fig. 2 do not account for photobleaching or ADP-mediated inhibition. Panel D shows optimized fit of the model to the fluorescence decay of the Hooijman et al. experiment (Fig. 2B) from Hooijman et al. [2]), demonstrating perfect match of the kinetic model to the observed data.

Panel A shows the simulated bulk state probabilities during the rigor, incubation, and chase phases of the experiment. During the incubation phase P_{A_2} rapidly drops from 40% to zero following the introduction of mant-ATP. The rapid drop in P_{A_2} is associated with a rapid spike in P_{D_T} at the beginning of the incubation phase. However, the D_T (DRX) state is predicted to rapidly hydrolyze to the D_D state. Thus P_D rises to nearly 100% at the beginning of the incubation phase. The distribution of probability into P_S (the occupancy probability of the SRX state) is gradual over the two-minute incubation and ten-minute chase phase. The DRX state probability P_{D_T} remains roughly 1000-fold lower than the SRX or D_D state probabilities throughout the incubation and chase phases, yet facilitates fine balance between SRX and DRX.

Panel B shows the corresponding predicted distribution of fluorescent label states during this experiment. During the incubation phase the fluorescent label accumulates primarily in the M_S and M_D states since the proportion of the system in the P_{D_T} state is relatively negligible. During the chase phase the decay of the M_D state represents the fast phase of fluorescent decay and the decay of the M_S state represents the slow phase. Using Equations (2) and (1) to assess the simulated data, or equivalently to assess the pseudo data (constructed from row 1, Table 1 of [2]) from Panel D, yields estimates of the slow

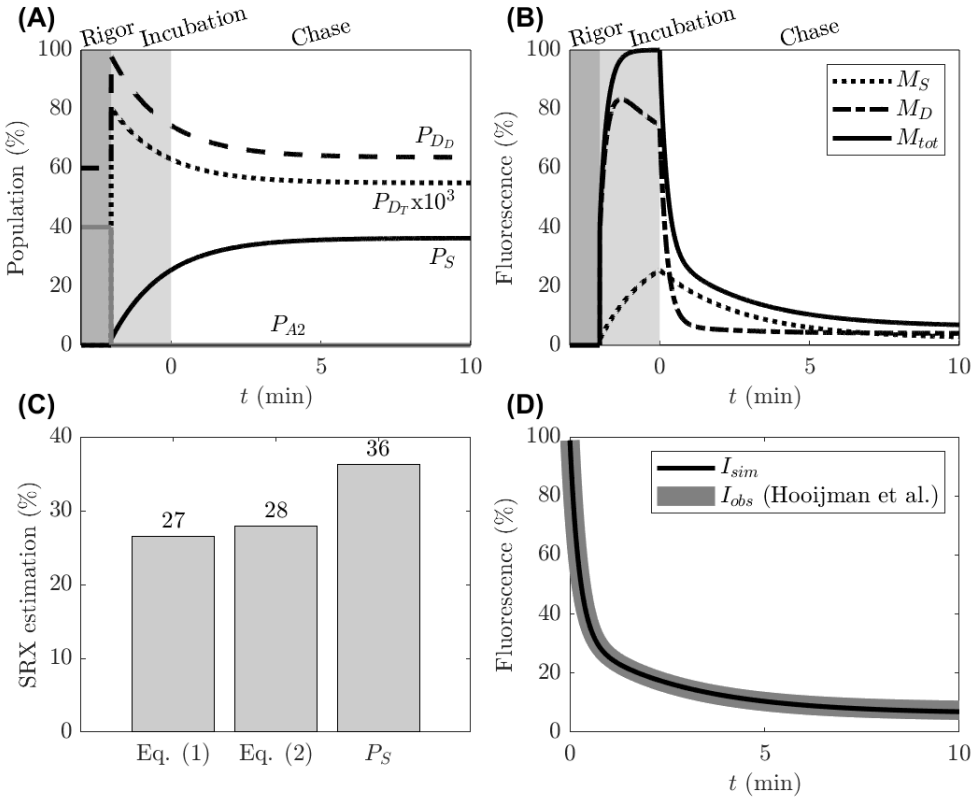

Fig 2. Simulation of the Hooijman et al. label-chase experiment with label incubation time of 2 minutes [2]. (A) The simulated state probabilities show transition from the attached rigor (A_2) and ADP-bound (P_D) states to the SRX (P_S) and ATP-bound DRX (P_{D_T}) states following addition of mant-ATP to initiate the label incubation phase. (B) The predicted kinetics of fluorescent labeled states shows that while the labeling reaches maximal capacity during the incubation phase, the label distribution between the D_D and SRX states has not reached steady state at the end of the incubation phase. (C) The estimated SRX fraction, based on fits of simulated data to Equations (1) and (2) is 27 and 28%, while the simulated steady-state probability of the SRX state is 36%. (D) Simulated fluorescent intensity I_{tot} during the chase phase perfectly reproduces the fluorescence decay in the ATP chase phase I_{obs} observed by [2].

phase fraction of 0.26 and 0.28, as illustrated in Fig. 2C. However, as indicated in Panels A and C, the long-time steady-state value of the P_S predicted from these simulations is 0.36. This discrepancy may contribute to differences in predictions of the SRX fraction made using different experimental protocols.

3.2 Analysis of the Walklate et al. Experiment

Model simulations fitting a sample stopped-flow experiment of Walklate et al. ([7], Fig 1D), using bovine masseter myofibrils, are illustrated in Fig. 3. The data are presented as in Walklate et al., Figure 1A, assuming normalized to maximum intensity of the loading phase. As for Fig. 2, simulations in Fig. 3 do not

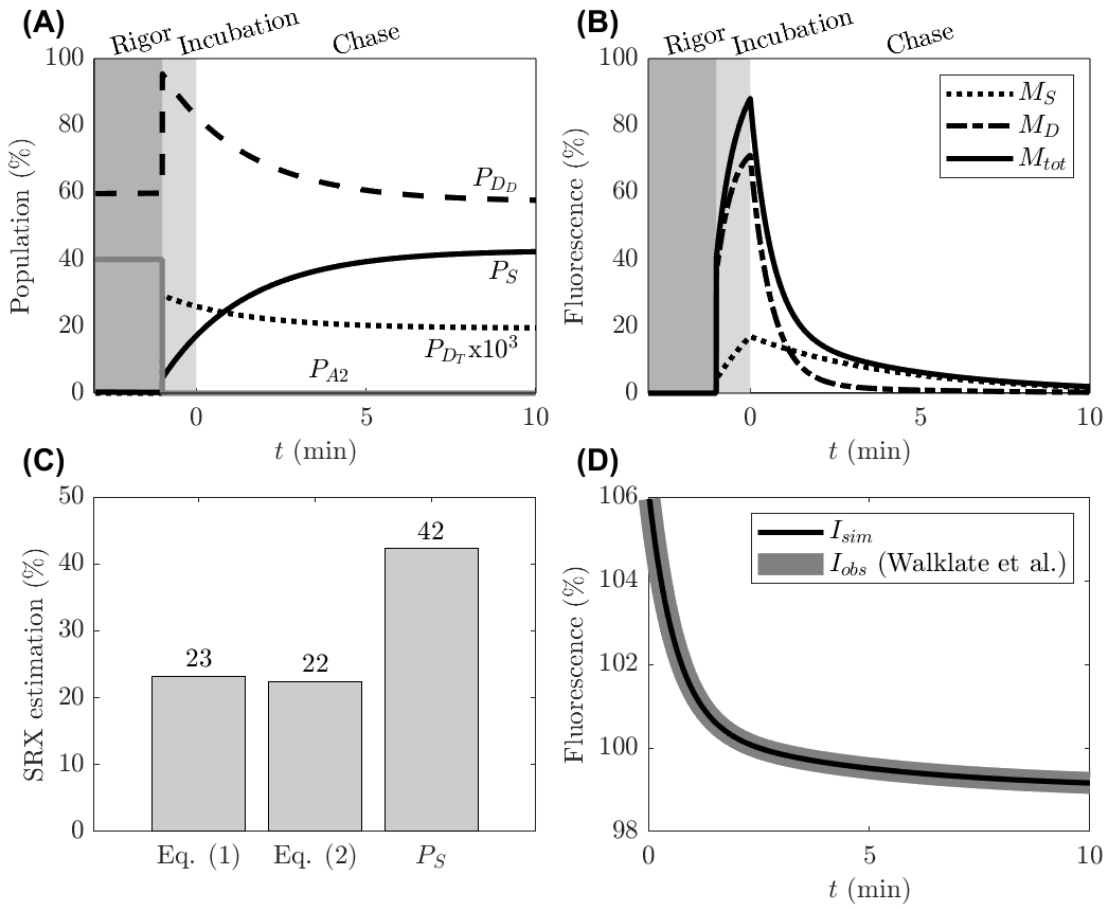

Fig 3. Simulation of the Walklate et al. sample experiment ([7], Fig. 1A) (A) The simulated state probabilities show transition from the attached rigor (A_2) and ADP-bound (P_D) states to the SRX (P_S) and ATP-bound DRX (P_{D_T}) states following addition of mant-ATP to initiate the label incubation phase. Notice shorter incubation (60 seconds) compared to Fig. 2 (B) The predicted kinetics of fluorescent labeled states shows unsaturated labeling during incubation time. (C) The estimated SRX fraction, based on fits of simulated data to Equations (1) and (2) is approximately 23%. The simulated steady-state probability of the SRX state is 42%. (D) Simulated fluorescent intensity I_{tot} during the chase phase is fit to reproduce the fluorescence decay in the ATP chase phase I_{obs} observed by [7] Fig. 1A.

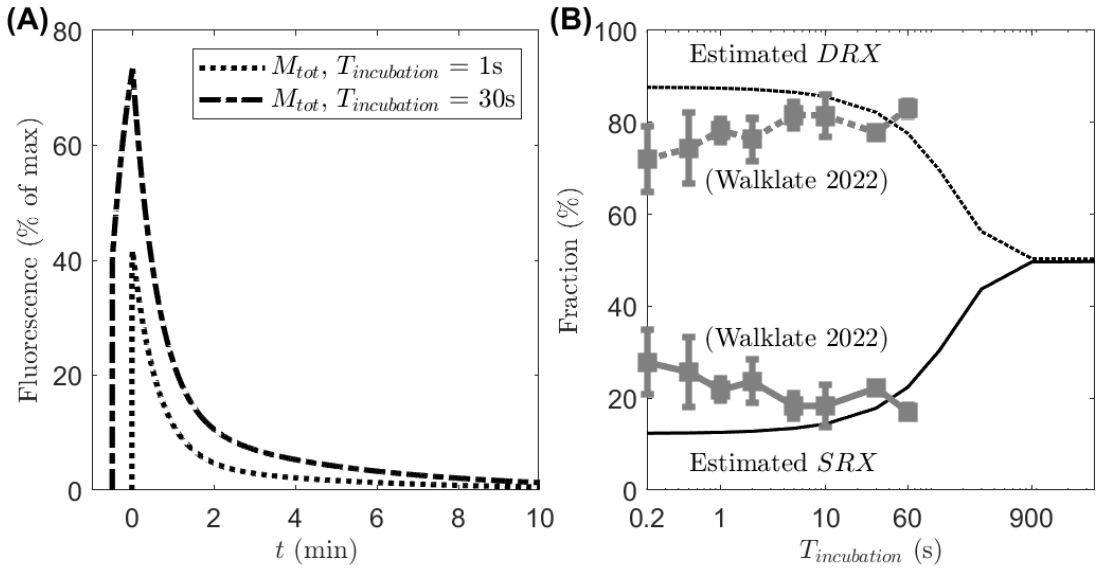

Fig 4. Effect of mant-ATP incubation time on estimated SRX and DRX fraction. A. Simulation of total mant label in the system for 1- and 30-second incubation time. B. Estimated SRX fraction from Equation (2) is plotted as a function of incubation time. (Estimated DRX fraction is 100% minus SRX fraction.) Data from Walklate et al. [7] Fig. 1D are shown for comparison.

account for photobleaching or ADP-mediated inhibition. Panel D demonstrates an essentially exact fit of the decay label, which is associated with an estimated SRX fraction of $P_s = 42\%$. However, as reported in panel C, fits to the decay to double exponential equations (Equations (1) and (2), yield estimate of 23%, approximately half of the value associated with the kinetic model that exactly matches the kinetic data.

Walklate et al. [7] observed that the slow decay phase during the chase phase of the experiment (attributed to the SRX state) is established with relatively short ($\approx$ 200 ms) incubation times. To explore this behavior we simulated a range of incubation times, from 0.2 seconds to 15 minutes, using the model parameters estimated based on Fig. 3. For each simulated incubation time, we simulated the chase phase and fluorescent decay, as in Fig. 3, and computed the estimated SRX fraction from Equation (2). Results are summarized in Fig. 4.

The left panel of Fig. 4 shows the predicted intensity time course for 1- and 30-second incubation times. For both incubation times, there is an initial effectively instantaneous loading of 40% of the total myosin states as the initial rigor fraction (here fixed at 40%) rapidly transitions to the D_T and subsequently the D_D state. Loading of the label slows following this initial fast phase and the magnitude of intensity reached for the 30-second incubation is greater than that for the 1-second incubation. However, the shapes of the decay curve during the chase phase are similar, showing similar bi-exponential behavior. Estimating the SRX fraction based on Equation (2) for the 1-second incubation simulation yields 13%. Estimating the SRX fraction based on Equation (2) for the 30-second incubation simulation yields 18%. Thus using Equation (2) to assess the SRX fraction from these simulated data sets predicts that the estimated slow phase fraction is largely independent of incubation time over this range of incubation times.

The right panel of Fig. 4 shows the results of analyzing simulated data obtained for a range of

incubation times using Equation (2) to assess the SRX fraction. Simulated results are compared to the data of Walklate et al . [7]. Similar to the results reported by Walklate et al . [7] the simulated analysis shows that the estimated SRX fraction remains effectively constant over a certain range of incubation times: Over the loading times of 0.2 to 10 seconds the estimated SRX fraction increases from 12% to 14%. However, the estimated SRX fraction increases to 22% for the 60 second incubation time, while the analysis of Walklate et al. [7] shows a decrease from approximately 28% at 0.2 seconds to 17% at the 60 second incubation time. At higher incubation times the estimated SRX fraction saturates at 50%. Most importantly, the true steady state SRX population $P_s = 42\%$ for the simulated model, regardless of incubation time.

These results illustrate how the estimated slow phase fraction may be largely independent of incubation time over a wide range of incubation time, yet fully consistent with our simple mass-action kinetic model. Discrepancies between simulations and data of Walklate et al. in Fig. 4B may derive in part of the effects of ADP-mediated inhibition of the $D_D \rightarrow D_T$ state transition, which are not accounted for in Fig. 4.

3.3 Accounting for ADP-Mediated Inhibition

Walklate et al. [7] suggest that a build-up mant-ADP becomes limiting for incubation times longer than 60 seconds in their experimental setup. ADP-mediated inhibtion of the $D_D \rightarrow D_T$ transition is modeled using Equation (10). Using this formulation, sample data from Walklate may be fit and analyzed using a range of values of K_i. Fig. 5D shows an example fit to the single-mixing chase phase decay, assuming $K_i = 0.5$ μM for the 1-minute incubation experiment. Panels A and B show the simulated time courses of state probabilities and label occupancy for this fit. At this level of ADP-mediated inhibition the predicted P_S at the end of the chase phase is 35%—slightly lower than the 42% value observed in Fig. 3 with no ADP inhibition.

Although ADP-mediated inhibition is predicted to reduce the SRX state probability P_S, it is predicted to have the no effect on the estimated slow phase fraction from the chase phase data. Fig. 5C shows the predicted effect of ADP-inhibition on SRX estimation at $K_i = 0.5$ μM as a function of incubation time for the Walklate et al. double-mixing incubation-sweep experiment. Incorporation of ADP inhibition leads to a slightly worse match to the data compared to Fig. 4B. Thus, the decrease in estimated slow phase fraction observed by Walklate et al. is not explained by ADP-mediated inhibition as represented in this kinetic model. As demonstrated in Fig. 2 and Fig. 3, the slow phase fraction estimated from Equations (1) or (2) does not necessarily correspond to relative occupancy of the SRX state. Moreover, this prediction demonstrates that a kinetic mechanism that decreases the relative occupancy of the SRX state can have no effect on the slow phase fraction estimated from the double-expondential analysis of the chase phase data.

3.4 Effect of Initial Rigor Fraction

During the muscle preparation, the muscle fibers are demembranated for several hours and stored in various solutions (protocols differ). While some studies explicitly report a pre-incubation step in rigor (ATP depleted) buffer, these details are not always reported. Simulations above assume a finite initial occupancy of the $A2$ rigor state before the incubation phase. Once ATP is introduced into the system, the myosin heads rapidly accumulate in the D_D state. In the simulations above, initial fraction of myosin population in rigor state ($A_{2,0}$) was set to 40%. To evaluate the effect of this parameter on the predicted steady-state SRX, we reoptimized the model fit to the data from Fig. 1A of Walklate et al. [7] for each of

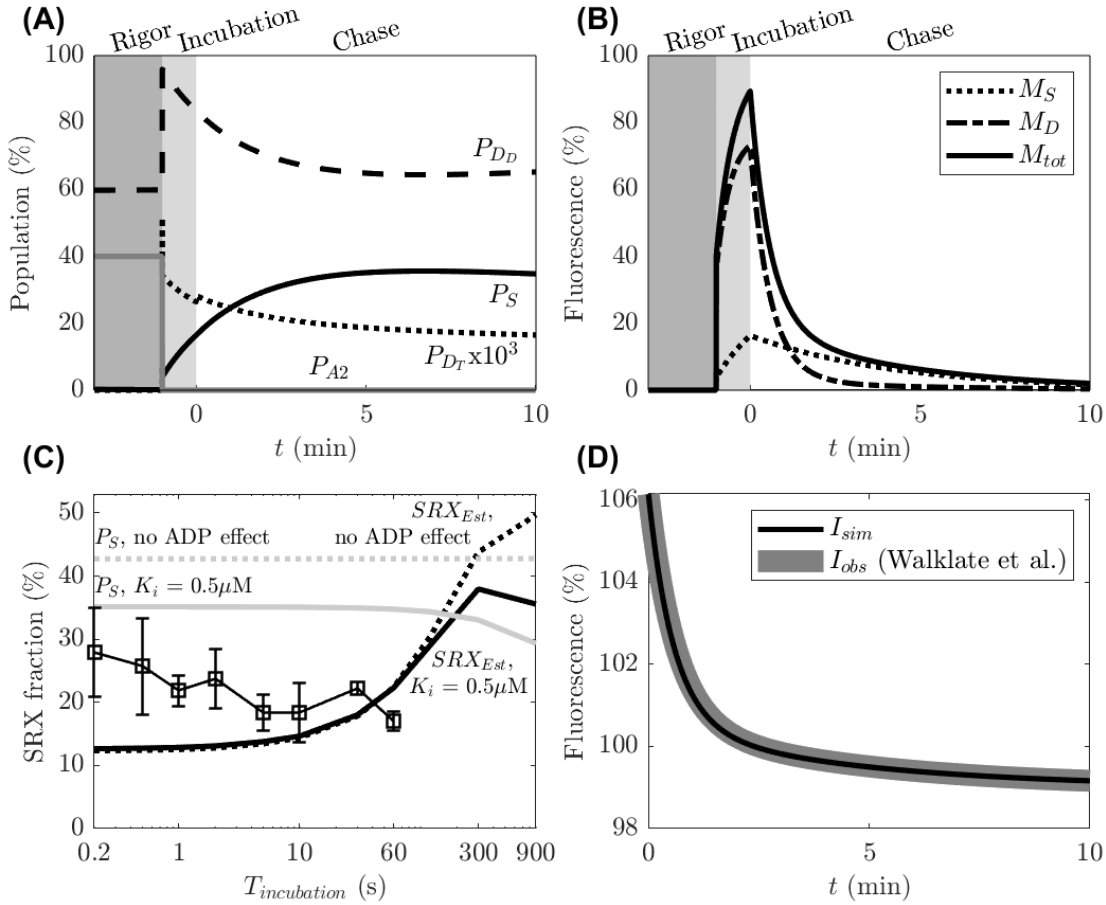

Fig 5. Simulation with ADP-dependent inhibition of $D_D \rightarrow D_T$ transition, with $K_i = 0.5$ μM. (A) The simulated state probabilities show that ADP-mediated inhibition leads to a lower steady-state SRX occupancy ($P_S = 35\%$ compared to 42% with no inhibition). (B) The predicted kinetics of fluorescent labeled states are equivalent to the simulated kinetics for the ADP-independent case of Figure 3. (C) The estimated SRX fraction, based on fits of simulated data to Equation (2) as a function in incubation time for the ADP inhbition case is nearly identical to the the ADP-independent case. (D) Simulated fluorescent intensity I_{tot} during the chase phase almost perfectly reproduces the fluorescence decay in the ATP chase phase I_{obs} observed by [7].

$A_{2,0} = (0, 20, 40, 60, 80, 100)$. Fig. 6D shows a fit to input data for $A_{2,0} = 80\%$, while panels A & B show the predicted state probabilities and label occupancy for this fit. Panel C shows the predicted steady-state SRX fraction, P_S, for the range of assumed $A_{2,0}$ values. While the value of $A_{2,0}$ has a large effect on the amount of label M_{tot} in the initial phase of the incubation (compare Fig. 3B and 6B), it has a minor observable effect on the predicted steady-state SRX fraction (Fig. 6C). In other words, all assumed values for $A_{2,0}$ result in the similar estimates for P_S, and model predictions in terms SRX occupancy are relatively insensitive to $A_{2,0}$.

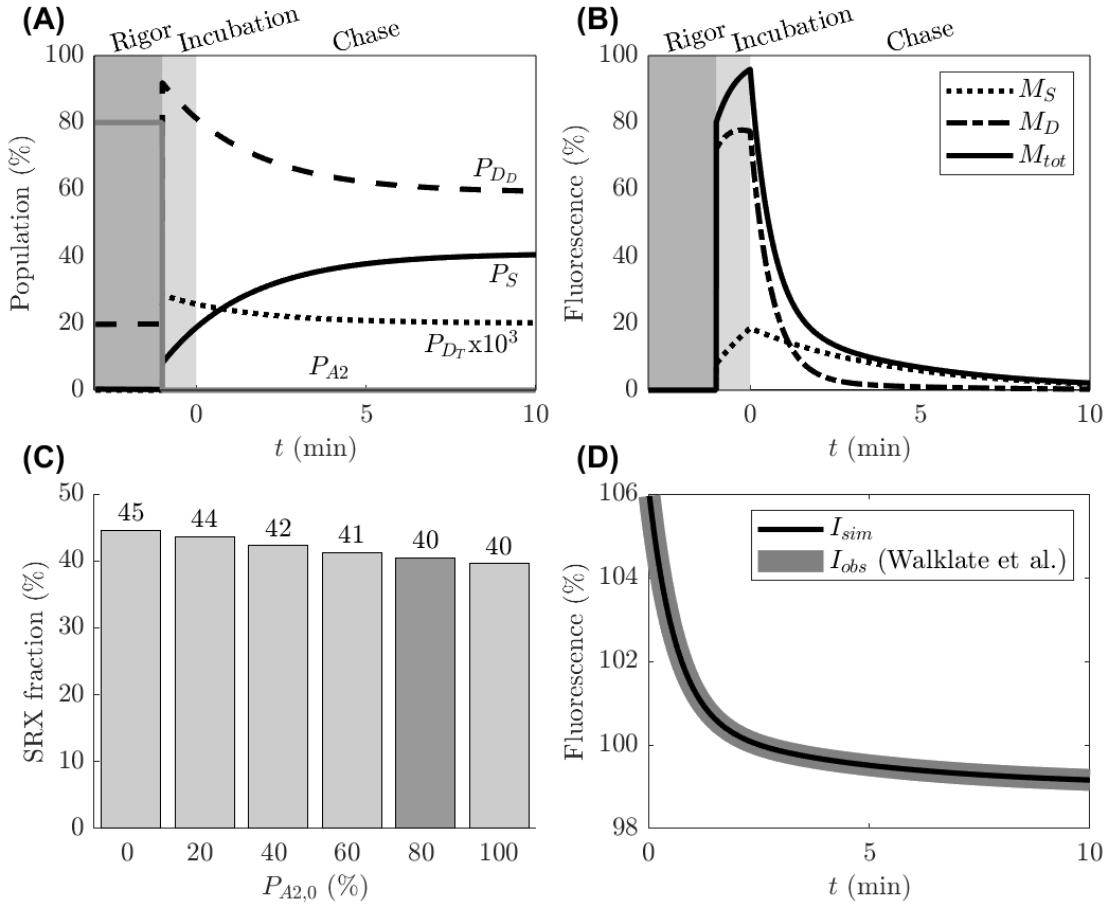

Fig 6. Effect of initial rigor fraction $A_{2,0}$, increased to 80%, on predicted steady-state SRX fraction. (A) The simulated state probabilities show transition from the attached rigor (A_2) and ADP-bound (P_D) states to the SRX (P_S) and ATP-bound DRX (P_{D_T}) states following addition of mant-ATP to initiate the label incubation phase (B) The predicted kinetics of fluorescent labeled states. (C) Different values of initial rigor state fraction $A_{2,0}$ yield little offect on predicted steady-state SRX fractions at larger $A_{2,0}$. (D) Simulated fluorescent intensity I_{tot} during the chase phase is fit to reproduce the fluorescence decay in the ATP chase phase I_{obs} observed by [7] Fig. 1A using $A_{2,0} = 80\%$.

3.5 Accounting for Photobleaching

Photobleaching via repeated excitation can gradually reduce the mant fluorescence signal by rending mant fluorophores unable to fluoresce. The photobleaching effect may be reduced through the experimental design (e.g. [6]) or accounted for in the data analysis (e.g. using a linear approximation, as in [13]). We evaluated the potential impact of photobleaching on predicted steady state SRX using the photobleaching model of Equation (9), which assumes a constant steady excitation and bleaching beginning at the start of the incubation phase.

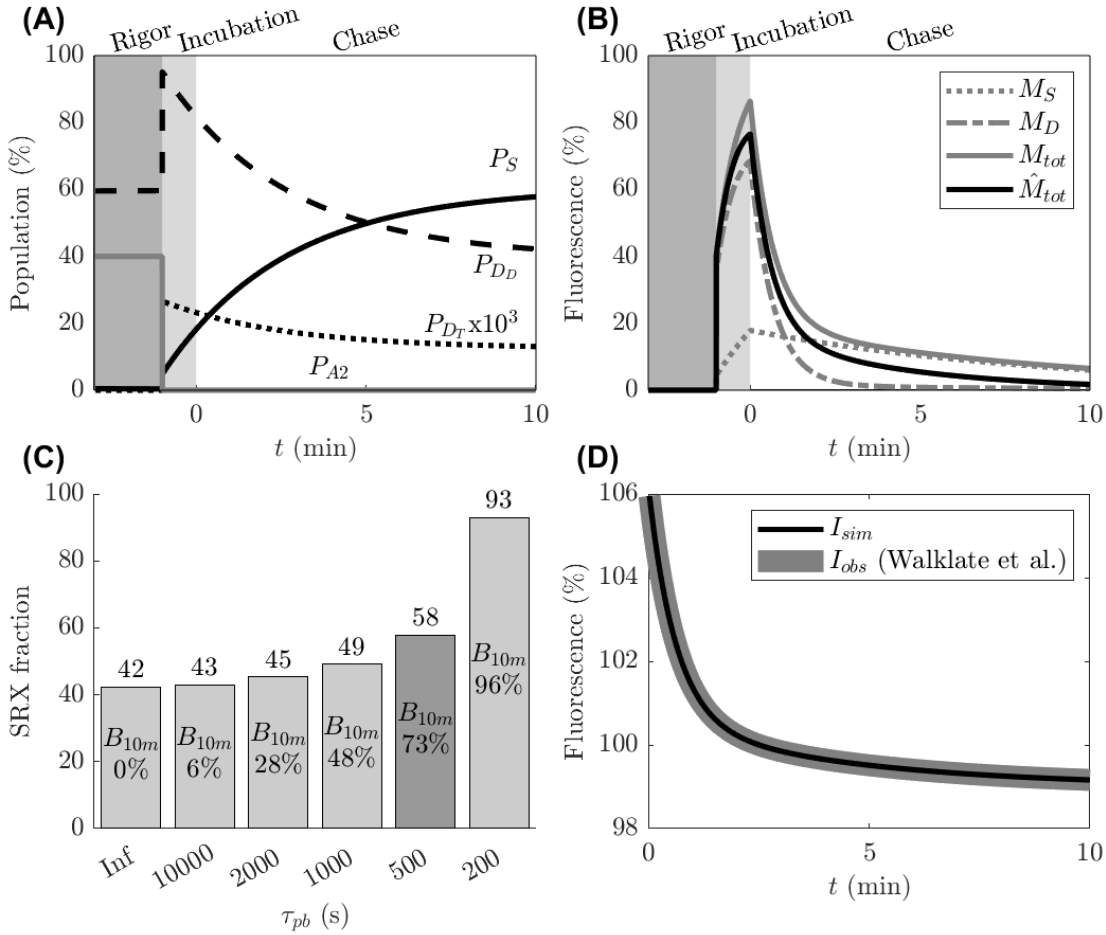

Fig 7. Effect of accounting for photobleaching on predicted SRX fraction, using $\tau_{pb} = 500$s. (A) The simulated state probabilities show transition from the attached rigor (A_2) and ADP-bound (P_D) states to the SRX (P_S) and ATP-bound DRX ($P_{D_{\hat{T}}}$) states (B) The predicted kinetics of fluorescent labeled states, with simulated photobleaching effect on $\hat{M}_{tot}$. (C) Different values of τ_{pb} yield different predicted steady-state SRX fractions, with $B_{10\mathrm{m}}$ indicating the relative attenuation of fluorescence at 10 minutes. (D) Simulated fluorescent intensity I_{tot} during the chase phase is fit to reproduce the fluorescence decay in the ATP chase phase I_{obs} observed by [7] Fig. 1A using $\tau_{pb} = 500$ seconds.

Fig. 7D shows a fit of the model to the data of Walklate et al. [7] assuming a photobleaching time constant of $\tau_{pb} = 500$ seconds. At this level of photobleaching the total fluorescent signal is attenuated by 73% by the end of the chase phase of the experiment. Panels A and B of Fig. 7 illustrate the state kinetics and fluorescent label kinetics predicted by the model for this fit to the data with $\tau_{pb} = 500$ seconds. The predicted steady-state SRX fraction, P_S, associated with this fit is 58%, greater than the 42% level obtained assuming no photobleaching. Panel C shows the predicted SRX fraction (the steady-state value of P_S) that is obtained for different values of τ_{pb}. Controlling for photobleaching is thus an important factor to consider for quantifying the SRX properly. We do not have a way of estimating the actual effects of

photobleaching on the data from the experiments analyzed here.

4 Discussion

We present a kinetic model of the myosin cross-bridge cycle and mant-ATP/ADP labeling to analyze the the observed kinetics of mant fluorescence in mant-ATP label/chase assays and to the biochemically defined SRX state of myosin. The model not only aligns with the available experimental data, but also provides a self-consistent explanation of three paradoxes summarized by Mohran et al. [6]. Namely, the model: (1) predicts a steady-state balance between the states that is compatible with myosin cross-bridge models, (2) demonstrates discrepancy between experimentally estimated SRX fraction using double exponential fit and the simulated steady-state SRX fraction, and (3) offers a novel interpretation of the experiment of Walklate et al. [7] where the apparent SRX fraction varies little over experiments using incubation times from 0.2 to 30 seconds.

Contemporary conceptual models of mant-ATP decay assume an independent exchange of ATP in both SRX and DRX states [2, 6]. Moreover, these models assume that both of these states undergo hydrolyzing exchange. That is, mant-ATP in both SRX and DRX can hydrolyze into mant-ADP + Pi, which may be replaced during the chase phase with unlabeled ATP. Our model is based on a fundamentally different kinetic scheme (Fig. 1), which is more consistent with existing models of the cross-bridge cycle. Also consistent with existing models of the cross-bridge cycle, our analysis predicts very low occupancy of the D_T state, consistent with a relatively rapid rate of ATP hydrolysis $D_T \to D_D$. However, even though the occupancy of the D_T state is very low, it is a critical part of the model—the relative flow of state probability from $D_T \to D_D$ to versus from $D_T \to S$ affects the P_S and P_D probabilities and thus governs the kinetics of the label/chase experiment.

Our analysis using this modeling framework reveals potential several important caveats for interpreting of mant-ATP label/chase experimental data:

1. Estimation of the SRX state occupancy based on double exponential analysis of the chase phase data, using either Equation (1) or (2), generally does not quantify the true fraction of the SRX state in steady state.

2. The SRX state is predicted to form relatively slowly (on the timescale of 5-10 minutes) during the incubation phase. Since predicted time for the SRX and DRX states to reach steady-state is significantly longer than commonly used incubation times, transition into the SRX state continues even after the fluorescence intensity is saturated (Fig. 2). The use of relatively short incubation times leads to significant underestimation of the true SRX state based on the quantification of the slow decay component of the chase phase time course.

3. Photobleaching may substantially affect the observed decay and interpretation, resulting in underestimating the true SRX of the muscle (Fig. 7).

The uncertainties associated with these caveats may be addressed through the experimental design and the data analysis approach. Most fundamentally, it is important to track and account for experimental details that are often ignored, including: the nature of the rigor incubation conditions, the incubation time, and the degree of photobleaching.

Our model assumes that ATP hydrolysis occurs only in the DRX state, via the $D_T \rightarrow D_D$ transition. However, more complex models may be conceived. For example, Fig. 8 illustrates an alternative model, where the SRX_{ATP} can hydrolyze into SRX_{ADP}. Using this model architecture we are able to match the label/chase experimental data as well as we are able to using the simpler model of Fig. 1A, albeit with more complexity and additional adjustable parameters (results not shown).

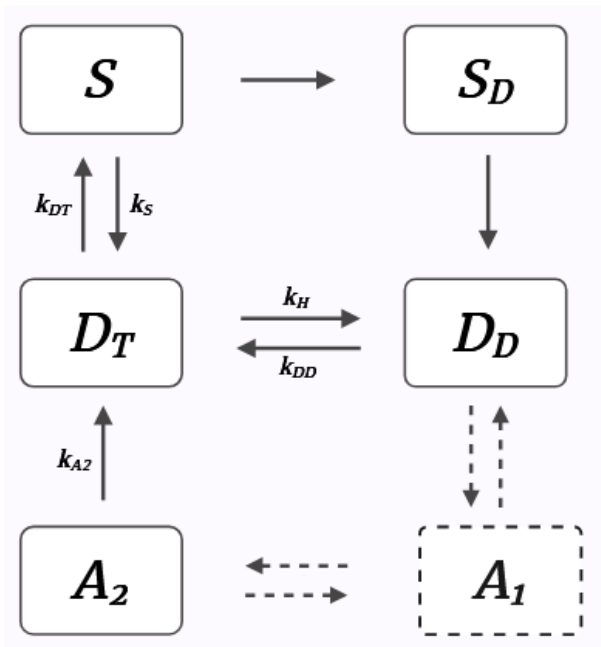

Fig 8. Alternative conceptual model. The SRX ATP-bound state S is allowed to hydrolyze to ADP-bound S_D state.

The presented model represents a simplification of complicated molecular processes in a kinetic model, ignoring important effects, including diffusion (recently elaborated by Montesel et al [14]), SRX recruitment affected by the muscle tone ([12]), temperature effects, non-specific mant- binding, measurement artifacts (e.g. background fluorescence, microscope focus) and potentially many others (see e.g. [15]). Thus, additional experiments may be required to take these effects into account.

The trend of decreasing SRX fraction with increasing loading time, as reported by Walklate et al. [7], cannot be reproduced by the current kinetic model—even when incorporating photobleaching and ADP accumulation effects. This discrepancy may reflect either experimental variability or the presence of biochemical factors not accounted for in the model. The observed decrease in variability in the data with longer incubation aligns with model predictions of increased label accumulation during the incubation phase (Fig. 4B). A lower amount of bound label at shorter incubation times implies a lower signal-to-noise ratio, which could contribute to higher measurement uncertainty.

5 Conclusion

Our analysis suggests that apparent paradoxical interpretations of the mant-ATP label/chase experiment to assess myosin states may be explained using a kinetic model, while accounting for potential protocol differences.

Application of this kinetic framework may improve the quantification and interpretation of the label/chase experiment. For example, we estimated the actual SRX fraction to be 42% in a representative stopped-flow experiment (Walklate et al., 2022), compared to the originally reported 22%, based on the slow-phase fraction double-exponential fit. The presented model may be be used for enhanced quantification of not only the SRX state occupancy, but also of the transition rates.

6 Acknowledgements

We appreciate a thoughtful discussion with Kenneth Campbell.

This work was supported by National Heart, Lung and Blood Institute Grants R01 HL154624 and R01 HL173346.

References

1. Stewart MA, Franks-Skiba K, Chen S, Cooke R. Myosin ATP turnover rate is a mechanism involved in thermogenesis in resting skeletal muscle fibers. Proc Natl Acad Sci U S A. 2010;107(1):430–435. doi:10.1073/pnas.0909468107.

2. Hooijman P, Stewart MA, Cooke R. A new state of cardiac myosin with very slow ATP turnover: a potential cardioprotective mechanism in the heart. Biophys J. 2011;100(8):1969–1976. doi:10.1016/j.bpj.2011.02.061.

3. Jani VP, Song T, Gao C, Gong H, Sadayappan S, Kass DA, et al. The structural OFF and ON states of myosin can be decoupled from the biochemical super- and disordered-relaxed states. PNAS Nexus. 2024;3(2):gae039. doi:10.1093/pnasnexus/pgae039.

4. Craig R, Padrón R. Structural basis of the super- and hyper-relaxed states of myosin II. J Gen Physiol. 2022;154(1). doi:10.1085/jgp.202113012.

5. Anderson RL, Trivedi DV, Sarkar SS, Henze M, Ma W, Gong H, et al. Deciphering the super relaxed state of human β-cardiac myosin and the mode of action of mavacamten from myosin molecules to muscle fibers. Proc Natl Acad Sci U S A. 2018;115(35):E8143–E8152. doi:10.1073/pnas.1809540115.

6. Mohran S, Kooiker K, Mahoney-Schaefer M, Mandrycky C, Kao K, Tu AY, et al. The biochemically defined super relaxed state of myosin-A paradox. J Biol Chem. 2024;300(1):105565. doi:10.1016/j.jbc.2023.105565.

7. Walklate J, Kao K, Regnier M, Geeves MA. Exploring the super-relaxed state of myosin in myofibrils from fast-twitch, slow-twitch, and cardiac muscle. J Biol Chem. 2022;298(3):101640. doi:10.1016/j.jbc.2022.101640.

8. Gollapudi SK, Ma W, Chakravarthy S, Combs AC, Sa N, Langer S, et al. Two classes of myosin inhibitors, para-nitroblebbistatin and mavacamten, stabilize β-cardiac myosin in different structural and functional states. J Mol Biol. 2021;433(23):167295. doi:10.1016/j.jmb.2021.167295.

9. Gollapudi SK, Yu M, Gan QF, Nag S. Synthetic thick filaments: A new avenue for better understanding the myosin super-relaxed state in healthy, diseased, and mavacamten-treated cardiac systems. J Biol Chem. 2021;296(100114):100114. doi:10.1074/jbc.RA120.016506.

10. Tewari SG, Bugenhagen SM, Palmer BM, Beard DA. Dynamics of cross-bridge cycling, ATP hydrolysis, force generation, and deformation in cardiac muscle. J Mol Cell Cardiol. 2016;96:11–25. doi:10.1016/j.yjmcc.2015.02.006.

11. Marzban B, Lopez R, Beard D. Computational modeling of coupled energetics and mechanics in the rat ventricular myocardium. Physiome. 2020;doi:10.36903/physiome.12964970.v1.

12. Campbell KS, Janssen PML, Campbell SG. Force-Dependent Recruitment from the Myosin Off State Contributes to Length-Dependent Activation. Biophys J. 2018;115(3):543–553. doi:10.1016/j.bpj.2018.07.006.

13. Patel JT, Belsham HR, Rathbone AJ, Friel CT. Use of stopped-flow fluorescence and labeled nucleotides to analyze the ATP turnover cycle of kinesins. J Vis Exp. 2014;(92):e52142. doi:10.3791/52142.

14. Montesel M, De Napoli C, Schmidt L, Germinario E, Guzman UH, Olsen JV, et al. A combined experimental and computational analysis of mantATP turnover in skinned muscle fibers. Proc Natl Acad Sci U S A. 2025;122(20):e2502652122. doi:10.1073/pnas.2502652122.

15. Nag S, Trivedi DV. To lie or not to lie: Super-relaxing with myosins. Elife. 2021;10. doi:10.7554/eLife.63703.

16. Ma W, Henze M, Anderson RL, Gong H, Wong FL, Del Rio CL, et al. The super-relaxed state and length dependent activation in porcine myocardium. Circ Res. 2021;129(6):617–630. doi:10.1161/CIRCRESAHA.120.318647.

17. Gordon AM, Regnier M, Homsher E. Skeletal and Cardiac Muscle Contractile Activation: Tropomyosin “Rocks and Rolls”. Physiology. 2001;16(2):49–55. doi:10.1152/physiologyonline.2001.16.2.49.